# The GPCR modulator protein RAMP2 is essential for angiogenesis and vascular integrity

Yuka Ichikawa-Shindo,[1] Takayuki Sakurai,[1] Akiko Kamiyoshi,[1] Hisaka Kawate,[1] Nobuyoshi Iinuma,[1] Takahiro Yoshizawa,[1] Teruhide Koyama,[1] Junichi Fukuchi,[1] Satoshi Iimuro,[2] Nobuo Moriyama,[3] Hayato Kawakami,[4] Toshinori Murata,[5] Kenji Kangawa,[6] Ryozo Nagai,[2] and Takayuki Shindo[1,7]

[1]Department of Organ Regeneration, Shinshu University Graduate School of Medicine, Nagano, Japan. [2]Department of Cardiovascular Medicine, University of Tokyo, Tokyo, Japan. [3]Department of Experimental Nursing, Faculty of Nursing, Fukuoka Prefectural University, Fukuoka, Japan. [4]Department of Anatomy, Kyorin University School of Medicine, Tokyo, Japan. [5]Department of Ophthalmology, Shinshu University Graduate School of Medicine, Nagano, Japan. [6]National Cardiovascular Center Research Institute, Osaka, Japan. [7]PRESTO, Japan Science and Technology Agency, Saitama, Japan.

**Adrenomedullin (AM) is a peptide involved both in the pathogenesis of cardiovascular diseases and in circulatory homeostasis. The high-affinity AM receptor is composed of receptor activity–modifying protein 2 or 3 (RAMP2 or -3) and the GPCR calcitonin receptor–like receptor. Testing our hypothesis that RAMP2 is a key determinant of the effects of AM on the vasculature, we generated and analyzed mice lacking RAMP2. Similar to AM$^{-/-}$ embryos, RAMP2$^{-/-}$ embryos died in utero at midgestation due to vascular fragility that led to severe edema and hemorrhage. Vascular ECs in RAMP2$^{-/-}$ embryos were severely deformed and detached from the basement membrane. In addition, the abnormally thin arterial walls of these mice had a severe disruption of their typically multilayer structure. Expression of tight junction, adherence junction, and basement membrane molecules by ECs was diminished in RAMP2$^{-/-}$ embryos, leading to paracellular leakage and likely contributing to the severe edema observed. In adult RAMP2$^{+/-}$ mice, reduced RAMP2 expression led to vascular hyperpermeability and impaired neovascularization. Conversely, ECs overexpressing RAMP2 had enhanced capillary formation, firmer tight junctions, and reduced vascular permeability. Our findings in human cells and in mice demonstrate that RAMP2 is a key determinant of the effects of AM on the vasculature and is essential for angiogenesis and vascular integrity.**

## Introduction

Many vasoactive substances play critical roles in the maintenance of cardiovascular homeostasis; moreover, imbalances among these substances have been implicated in the pathogenesis of various cardiovascular diseases. Among these, adrenomedullin (AM) was originally identified as a vasodilating peptide isolated from human pheochromocytoma (1) and, based on its structural homology and similar vasodilatory effects, has been classified as a member of the peptide family that also includes calcitonin gene–related peptide (CGRP). Although produced by a variety of tissues and cell types, AM is primarily secreted by vascular cells and functions as a local autocrine or paracrine (2) mediator, as well as a circulating hormone (3). Apart from its vasodilatory effect, AM also exerts diuretic (4) and cardiotonic (5) effects and is involved in the regulation of hormone release (6, 7), inflammation (8), and oxidative stress (9, 10) as well as the proliferation, migration, and differentiation of various cell types (11–13). Thus, AM is now recognized to be a pleiotropic vasoactive molecule. To better understand the in vivo functions of AM, we established and analyzed genetically engineered AM-deficient mice (14–25). Homozygous AM KO (AM$^{-/-}$) mice die

in utero at around midgestation from systemic hemorrhage and edema resulting from the fragility of their vasculature (14). In addition to mediating vascularization during development, we found that AM also enhances revascularization in adult tissues subjected to ischemia (25). The potential clinical applications of AM implied by these findings have attracted much attention, with particular attention being paid to AM's ability to stimulate vascular regeneration in ischemic tissue (26, 27).

AM signaling is regulated by a unique control system (28–31). The AM receptor is a 7–transmembrane domain GPCR named calcitonin receptor–like receptor (CRLR). CRLR associates with an accessory protein, receptor activity–modifying protein (RAMP), which is composed of about 160 amino acids and includes a single membrane-spanning domain. So far, 3 RAMP subtypes have been identified. By interacting with RAMP1, CRLR acquires a high affinity for CGRP, whereas by interacting with either RAMP2 or RAMP3, CRLR acquires a high affinity for AM. This novel system enables CRLR to transduce the signals of multiple ligands, although the precise mechanism remains largely unknown.

We hypothesized that not only the receptor-ligand specificity, but also the diversity, of AM's biological activities reflects its novel regulation by RAMPs. To test this idea, we generated RAMP2 KO mice, which were then used to analyze the physiological functions of the AM-RAMP2 system.

## Results

*Generation of RAMP2-null mice.* We initially analyzed the expression of AM and its related genes during midgestational development (E11.5–E14.5),

---

**Nonstandard abbreviations used:** AGM, aorta-gonad-mesonephros; AM, adrenomedullin; CDN5, claudin 5; CGRP, calcitonin gene–related peptide; CRLR, calcitonin receptor–like receptor; RAMP, receptor activity–modifying protein; RAMP2O/E, RAMP2-overexpressing (cell); ZO-1, zona occludens–1.

**Conflict of interest:** The authors have declared that no conflict of interest exists.
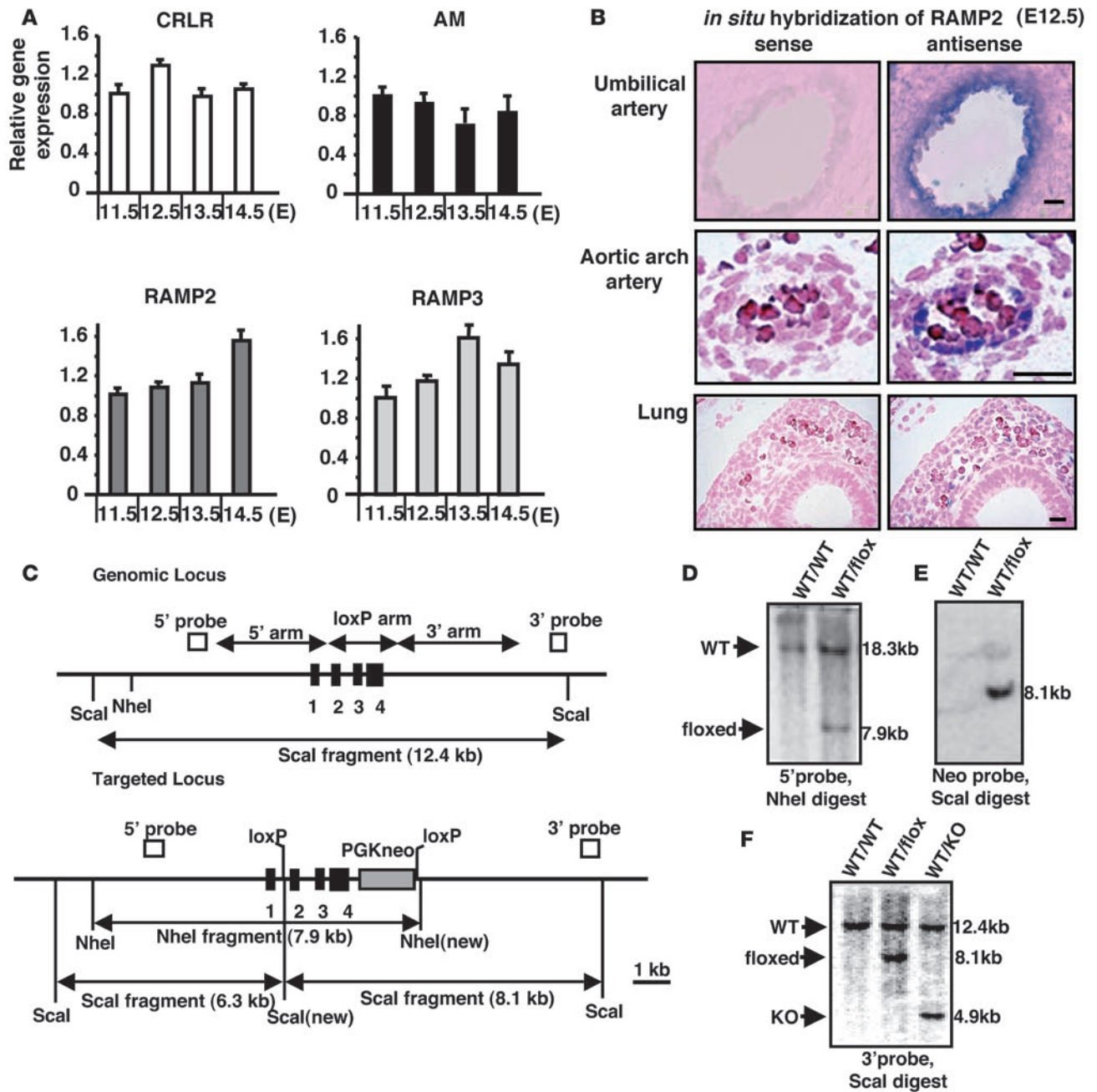
**Figure 1**

RAMP2 expression during development and generation of RAMP2 knockout mice. (**A**) Real-time PCR analysis of gene expression during E11.5–E14.5 in WT embryos. Expression is shown relative to that at E11.5. n = 5 per time point. AM, CRLR and RAMPs were expressed during midgestation. (**B**) In situ hybridization of *RAMP2* in WT embryos. Sections of umbilical artery, aortic arch, and lung from E12.5 WT embryos were used. Intense RAMP2 expression was detected in the vascular ECs. Scale bars: 20 μm. (**C**) Targeted disruption of mouse *RAMP2*. The genomic locus and predicted targeted locus are shown. Boxes denote exons 1–4 of RAMP2; ScaI and NheI restriction sites and loxP sites are indicated. Probes for Southern blot analysis are shown. (**D–F**) Southern blot analysis of mouse genomic DNA. (**D**) DNA was digested with NheI and probed with the 5′ probe. The 7.9-kb and 18.3-kb fragments denote floxed and WT alleles, respectively. (**E**) DNA was digested with ScaI and probed with the Neo probe. The 8.1-kb fragment denotes flox. (**F**) DNA was digested with ScaI and probed with the 3′ probe. The 8.1-kb ScaI fragment denotes flox; the 12.4-kb fragment denotes WT. The 4.9-kb fragment denotes the KO allele, generated by deletion of the loxP site using Cre recombinase.

the stage at which $AM^{-/-}$ embryos typically die. We found that in WT mice, AM, CRLR, RAMP2, and RAMP3 all continued to be expressed at midgestation (Figure 1A), which is consistent with previous findings (32, 33). Using in situ hybridization, we detected AM expression

in the vascular system (data not shown) and found that, among the RAMPs, only RAMP2 was specifically expressed in the vasculature at that stage (Figure 1B). We therefore speculated that it is RAMP2 that determines AM's function during vascular development and pro-

**Table 1**
Genotype of embryos from *RAMP2+/−* male and female mouse intercrosses

| Stage | Incidence (*n*) | | | Total |
|-------|-----------------|--|--|-------|
| | *RAMP2+/+* | *RAMP2+/−* | *RAMP2−/−* | |
| E11.5 | 5 | 11 | 6 | 22 |
| E12.5 | 31 | 58 | 29 | 118 |
| E13.5 | 22 | 50 | 24[A] | 96 |
| E14.5 | 13 | 26 | 13[B] | 52 |

[A]Of these, 3 embryos were dead. [B]Of these, 12 embryos were dead.

ceeded to generate RAMP2-specific KO mice to directly assess the functions of the AM-RAMP2 system in vivo.

The targeting strategy and analysis of homologous recombination are shown in Figure 1, C–F. RAMP2 heterozygous KO mice (*RAMP2+/−*) were apparently normal, although the number of live births was markedly diminished when *RAMP2+/−* mice were intercrossed. No RAMP2 homozygous KO (*RAMP2−/−*) newborns were obtained, and analysis of the embryos from timed *RAMP2+/−* intercrosses showed that the *RAMP2−/−* genotype was lethal at midgestation. The mortality rate among *RAMP2−/−* embryos was 13% at E13.5, 92% at E14.5, and 100% at E15.5 (Table 1). The most lethal stage (E13.5–E14.5) was nearly identical to that of the *AM−/−* genotype.

Real-time PCR analyses (Figure 2A) showed there to be no expression of RAMP2 in *RAMP2−/−* embryos, confirming that the *RAMP2* gene was successfully destroyed. By contrast, expression of RAMP3 did not differ in *RAMP2−/−* and WT mice, which indicates that no functional redundancy exists between RAMP2 and RAMP3 during development. Moreover, the expression of AM was upregulated by more than 5-fold in *RAMP2−/−* mice, presumably as a compensatory response to the absence of a functional AM receptor.

*Macroscopic and histological observation of RAMP2−/− embryos.* At E13.5, well-developed vitelline arteries were detected on the yolk sacs of WT embryos, whereas *RAMP2−/−* embryos had only poorly developed vitelline arteries (Figure 2, B–D). Histological examination revealed that the vitelline arteries from *RAMP2−/−* embryos were smaller than those from WT embryos and appeared disorganized (Figure 2, E–H). That these phenotypes resembled those of *AM−/−* embryos (14) showed that deletion of RAMP2 was sufficient to reproduce the major phenotypes of the vascular abnormality seen in *AM−/−* mice. In *RAMP2−/−* embryos, moreover, some of the ECs in the vitelline (Figure 2, I and J) and umbilical (Figure 2, K and L) arteries appeared apoptotic.

As for the embryos, the most apparent finding in *RAMP2−/−* mice was severe systemic edema (Figure 2, M and N). They also showed accumulation of pericardial effusion suggestive of cardiac failure (Figure 2, O–R), and some had bleeding that was observable under the skin (Figure 2S) and within organs (Figure 2U). These phenotypes were also observed in *AM−/−* embryos (14), although *RAMP2−/−* mice showed systemic edema much more severe than that in *AM−/−* mice.

*Vascular abnormalities and gene expression in RAMP2−/− mice.* To determine whether the developmental abnormalities described above were the cause of the vascular fragility seen in *RAMP2−/−* embryos, we analyzed in detail the vascular structure at E12.5. Electron microscopic observation of the ECs of the vitelline arteries in *RAMP2−/−* embryos revealed deformity and detachment from the basement membrane

(Figure 3B). Similar EC detachment was also detected in the liver (Figure 3D). In addition, there was abnormal thinning of the arterial walls in *RAMP2−/−* embryos (WT, 1.75 ± 0.12 μm; *RAMP2−/−*, 1.36 ± 0.05 μm; *P* < 0.05, *n* = 5 per group; Figure 3F), and the multiple layers of smooth muscle cells and basement membrane that normally comprise arterial walls were severely disrupted in *RAMP2−/−* embryos (Figure 3H). We also found that expression of molecules involved in cell adhesion was altered in arteries from *RAMP2−/−* mice. In particular, expression of vascular endothelial cadherin (VE-cadherin), claudin 5 (CDN5), and type IV collagen was diminished compared with WT mice (Figure 3I). These molecules are all important for the composition of tight junctions, adherence junctions, and the basement membrane of vascular ECs, and abnormalities involving them lead to paracellular leakage from the vascular lumen, which likely explains the severe edema seen in *RAMP2−/−* mice.

*Mechanisms underlying the angiogenesis and vascular stability mediated by the AM-RAMP2 system.* To analyze the mechanisms underlying the angiogenesis and vascular stability mediated by RAMP2, we next generated EC lines that stably overexpressed RAMP2 (RAMP2O/E cells), utilizing EAhy926 ECs (Figure 4, A and B; see Methods for details). EAhy926 ECs are known to form capillary-like tubes on Matrigel (34, 35). We observed that RAMP2O/E cells showed much greater capillary formation than did control cells in Matrigel assays (Figure 4, C–E), clearly demonstrating that upregulation of the AM-RAMP2 system enhances angiogenesis.

We then assessed endothelial barrier function by assaying vascular permeability in vitro. Cells were seeded onto semipermeable membranes in permeability chambers, after which the passage of FITC-dextran through confluent EC monolayers was monitored. Monolayers of RAMP2O/E cells were significantly less permeable than those of control cells, which suggests that upregulation of the AM-RAMP2 system also enhances vascular barrier function and reduces permeability (Figure 4F). We hypothesized that the reduced permeability reflected the firmer structure of the tight junctions formed by RAMP2O/E cells. To test this idea, we treated RAMP2O/E and control cells with $H_2O_2$ (0.5 mM), which leads to formation of intercellular gaps and reduced tight junction formation between ECs. Subsequent immunostaining of the tight junction marker zona occludens–1 (ZO-1) revealed that the structure was better preserved in RAMP2O/E than control cells (Figure 4, G–K). In addition, MTT and TUNEL assays revealed that RAMP2O/E cells showed significantly better viability after $H_2O_2$-induced damage than did control cells (data not shown).

We also found that expression of eNOS, VEGF, and CDN5 was upregulated in the RAMP2O/E cells and that treatment with the PI3K inhibitor LY294002 or a PKA inhibitor blocked those effects (Figure 4L). Thus, signaling via a PI3K- and PKA-dependent pathway appears to play a key role in AM-RAMP2 mediated angiogenesis and vascular stability. By contrast, RAMP3O/E cells did not show either enhanced angiogenesis or changes in permeability (data not shown). Apparently, the vascular functions of AM are exclusively regulated by RAMP2.

*Reduced responses to angiogenic stimuli in adult RAMP2+/− mice.* Unlike their homozygous KO littermates, *RAMP2+/−* mice survived until adulthood and were fertile, though aortic expression of RAMP2 was reduced to about half that seen in WT mice (Figure 5A), and they had higher BP than did WT mice (systolic BP, WT, 102.8 ± 2.2 mmHg; *RAMP2+/−*, 112.9 ± 2.2 mmHg; *P* < 0.01, *n* = 9 per group). With acute infusion of AM (10 nmol/kg), *RAMP2+/−* mice showed a smaller BP response than WT mice (maximum percent change in systolic BP,
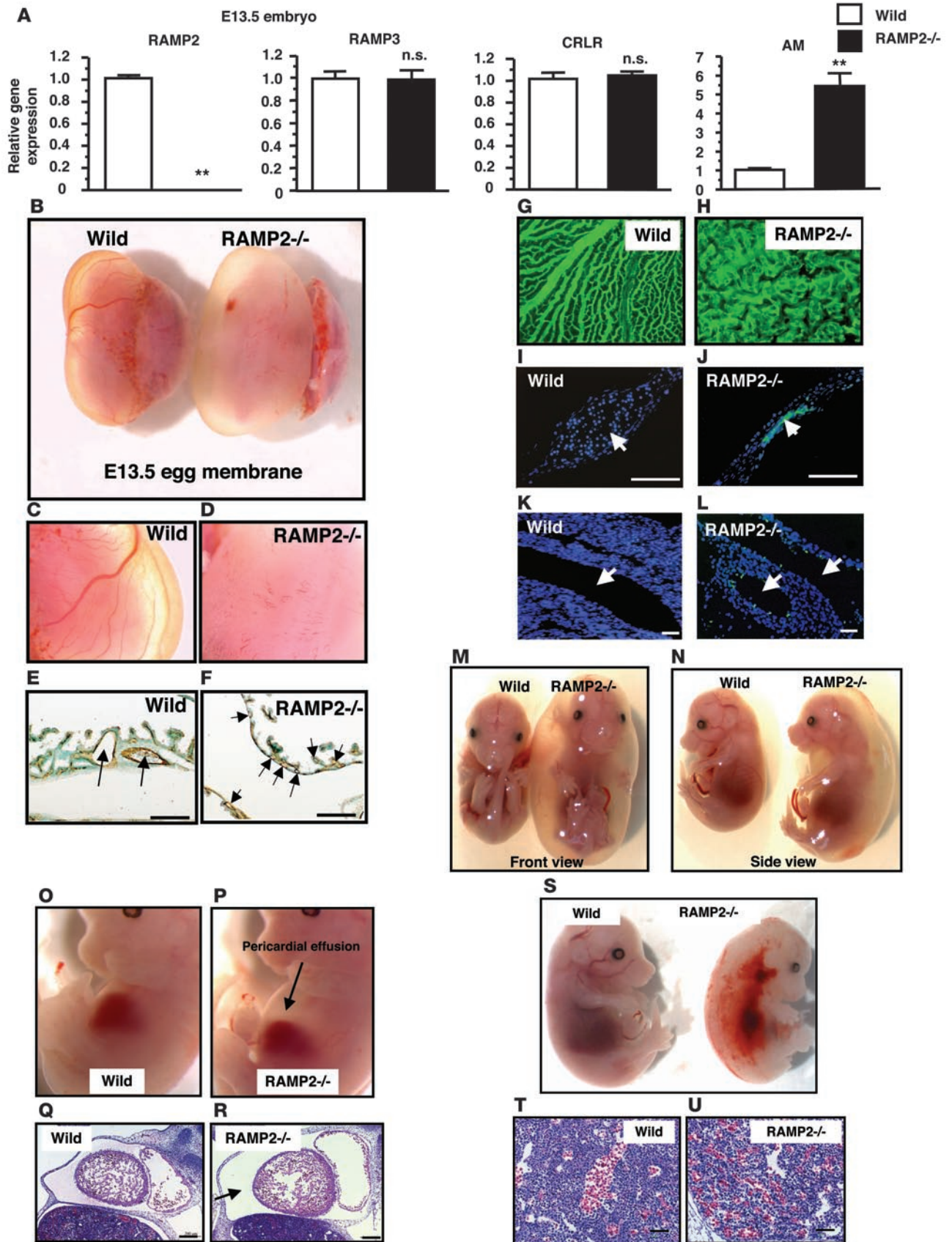
**A** E13.5 embryo

RAMP2 · RAMP3 n.s. · CRLR n.s. · AM **

Wild / RAMP2-/-

Relative gene expression

**B** Wild — RAMP2-/-
E13.5 egg membrane

**C** Wild · **D** RAMP2-/-

**E** Wild · **F** RAMP2-/-

**G** Wild · **H** RAMP2-/-

**I** Wild · **J** RAMP2-/-

**K** Wild · **L** RAMP2-/-

**M** Wild RAMP2-/- Front view · **N** Wild RAMP2-/- Side view

**O** Wild · **P** RAMP2-/- Pericardial effusion

**Q** Wild · **R** RAMP2-/-

**S** Wild RAMP2-/-

**T** Wild · **U** RAMP2-/-

**Figure 2**

Quantitative real-time PCR analysis, macroscopic analysis, and histology of $RAMP2^{-/-}$ embryos. (**A**) Gene expression of AM, CRLR, and RAMPs in E13.5 WT and $RAMP2^{-/-}$ embryos, assessed by real-time PCR of total RNA. No RAMP2 expression was detected in $RAMP2^{-/-}$ mice, confirming $RAMP2$ was successfully destroyed. Conversely, RAMP3 expression did not differ between $RAMP2^{-/-}$ and WT mice, showing that the absence of RAMP2 did not induce compensatory upregulation of RAMP3 during development. AM expression was upregulated more than 5-fold in $RAMP2^{-/-}$ mice. $n = 6$ per group. **$P < 0.01$ vs. WT. (**B**–**L**) Development of blood vessels in E13.5 WT and $RAMP2^{-/-}$ mice. Appearance of the yolk sac (**B**) and vitelline arteries (**C** and **D**). (**E** and **F**) CD31 immunostaining of sections of yolk sacs. Arrows indicate sections of vitelline arteries. (**G** and **H**) Whole-mount immunofluorescence staining of CD31 in yolk sacs. In **C**–**H**, vitelline arteries were well developed on the yolk sacs of WT mice but poorly developed on those of $RAMP2^{-/-}$ mice. (**I**–**L**) TUNEL staining of sections of vitelline artery (**I** and **J**) and umbilical vessel (**K** and **L**) in E13.5 WT and $RAMP2^{-/-}$ embryos. Apoptosis was visualized in green fluorescence. Arrows indicate vessel lumens. Some ECs in $RAMP2^{-/-}$ mice were TUNEL positive. (**M** and **N**) Severe systemic edema observed in $RAMP2^{-/-}$. Front (**M**) and side (**N**) views of WT and $RAMP2^{-/-}$ embryos at midgestation. Some $RAMP2^{-/-}$ embryos showed severe systemic edema. (**O**–**R**) Pericardial effusion in $RAMP2^{-/-}$ mice. (**O** and **P**) Magnified side view of embryos at midgestation revealing the appearance of the pericardial space in $RAMP2^{-/-}$ embryos. (**Q** and **R**) Sagittal sections showing the pericardial space in embryos at midgestation. The pericardial space was larger in $RAMP2^{-/-}$ than WT embryos and showed the accumulation of pericardial effusion. (**S**–**U**) Severe hemorrhagic changes in $RAMP2^{-/-}$ mice. (**S**) Side view of WT and $RAMP2^{-/-}$ embryos at midgestation. (**T** and **U**) Sections of the liver at the same stage. Some $RAMP2^{-/-}$ embryos showed severe hemorrhagic changes that were apparent on their surface and within the liver. Scale bars: 20 μm (**E** and **F**); 50 μm (**I**–**L**, **T**, and **U**); 200 μm (**Q** and **R**).

WT, 18.4 ± 1.4 mmHg; $RAMP2^{+/-}$, 13.3 ± 1.3 mmHg; $P < 0.05$, $n = 6$ per group). In contrast, CGRP-induced depressor effects did not differ in $RAMP2^{+/-}$ and WT mice (maximum percent change in systolic BP, WT, 15.9 ± 1.2 mmHg; $RAMP2^{+/-}$, 14.4 ± 1.3 mmHg; NS, $n = 6$ per group). Interestingly, AM expression was significantly upregulated in the aortas of $RAMP2^{+/-}$ mice, which suggests that reducing the num-

ber of functional AM receptors caused a compensatory upregulation of AM expression and implies that the AM-RAMP2 system is also important in the vascular function of adults. This prompted us to analyze the angiogenic properties of the AM-RAMP2 system in adult mice. We found that aortic ring explants cultured in collagen gel sprouted microvessels when stimulated with VEGF and that this
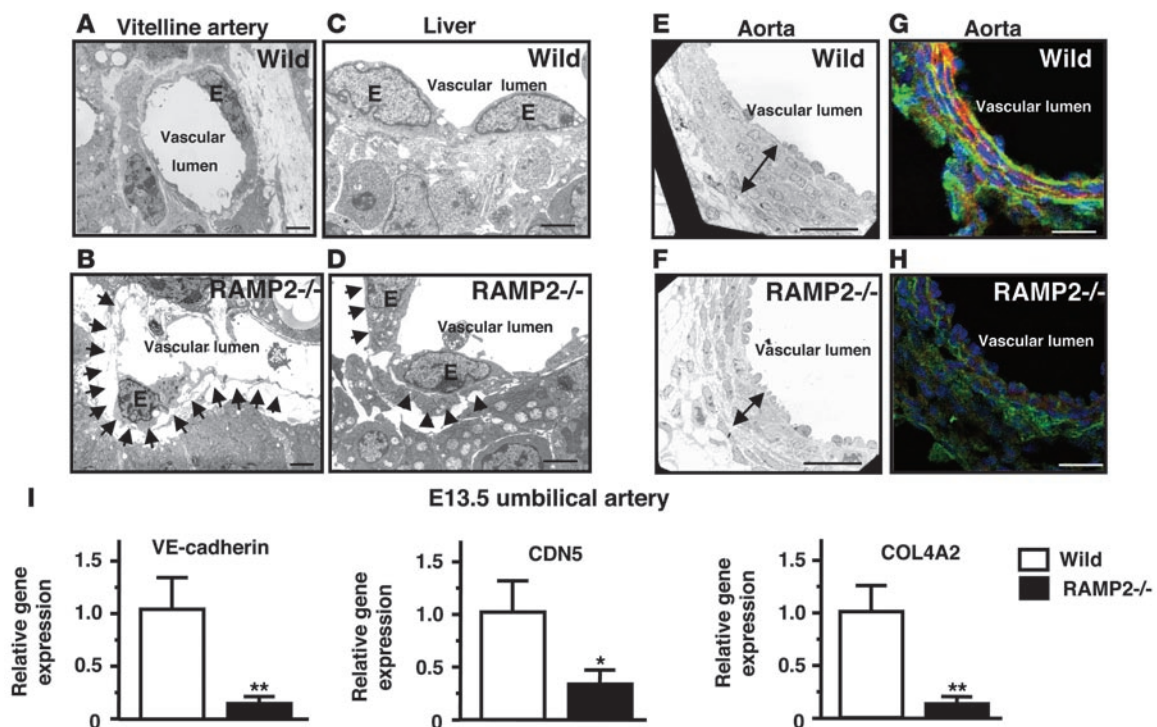


**Figure 3**

Abnormalities of vascular structure and gene expression in $RAMP2^{-/-}$ embryos. (**A**–**H**) Vascular structure of WT and $RAMP2^{-/-}$ embryos. Transmission electron micrographs of vitelline arteries (**A** and **B**), hepatic vessels (**C** and **D**), and aortas (**E** and **F**) from E12.5 $RAMP2^{-/-}$ and WT embryos. The vitelline arteries and hepatic vessels from $RAMP2^{-/-}$ mice showed the detachment of ECs (E) from basement membrane (arrows, **B** and **D**). In aortas from $RAMP2^{-/-}$ mice, the smooth muscle cell layer was thinner and rougher than in aortas from WT mice (double-headed arrows, **E** and **F**). (**G** and **H**) Immunohistochemical staining for type IV collagen and actin in aortas from WT and $RAMP2^{-/-}$ mice. Green, immunohistochemical staining using anti–mouse type IV collagen antibody; red, phalloidin (actin); blue, DAPI (nuclei). The structure of the smooth muscle cell layer and the basement membrane showed severe deformity in $RAMP2^{-/-}$ mice. (**I**) Quantitative real-time PCR analysis of gene expression in the umbilical artery from E13.5 embryos. Expression levels are shown relative to the level in WT embryos. VE-cadherin, CDN5, and α2 type IV collagen (COL4A2) expression was reduced in arteries from $RAMP2^{-/-}$ mice. $n = 6$ per group. *$P < 0.05$, **$P < 0.01$ vs. WT. Scale bars: 2 μm (**A**–**D**); 25 μm (**E**–**H**).
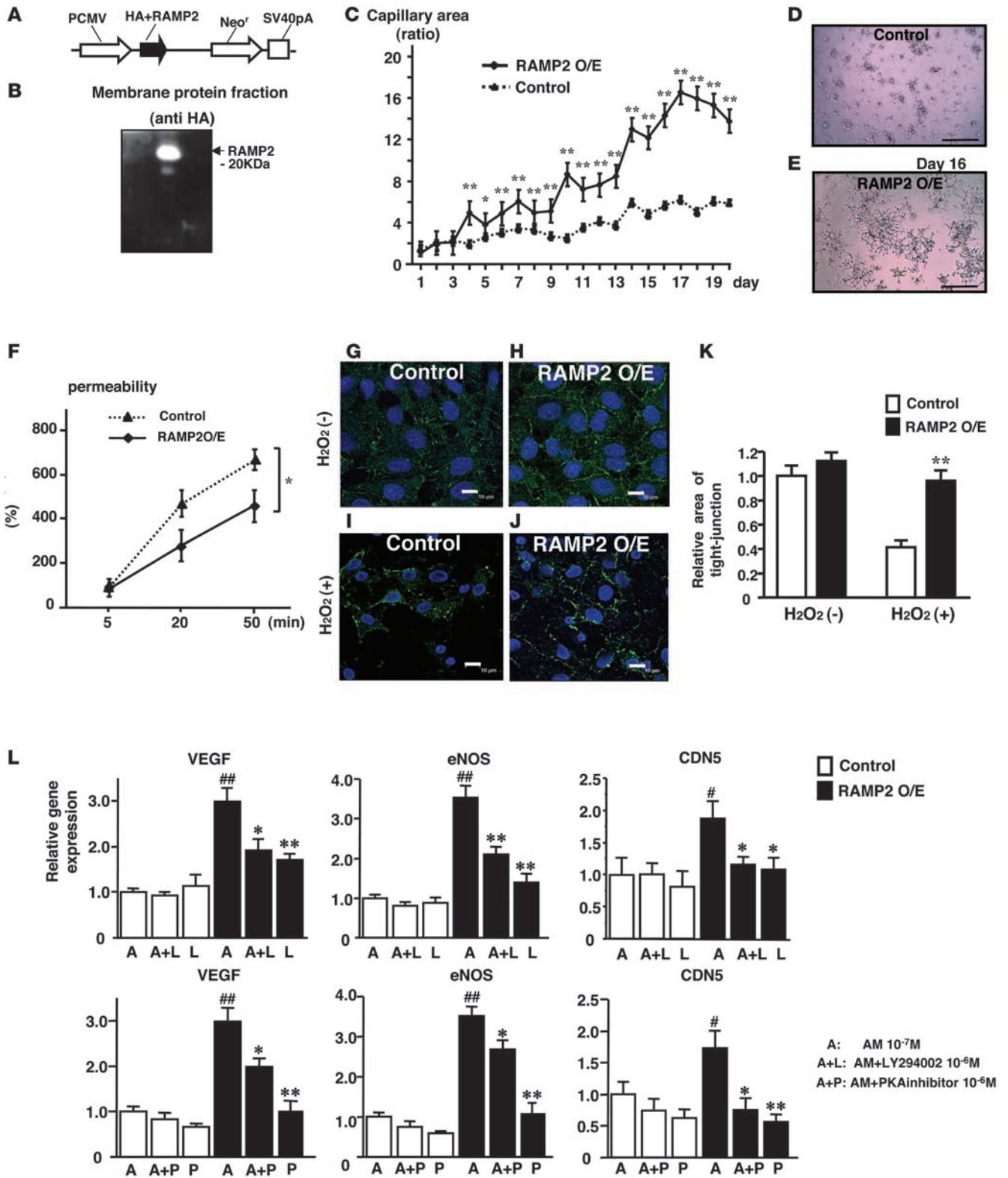
**A** PCMV  HA+RAMP2  Neo$^r$  SV40pA

**B** Membrane protein fraction
(anti HA)
← RAMP2
- 20KDa

**C** Capillary area (ratio)
- RAMP2 O/E
- Control

**D** Control

**E** Day 16  RAMP2 O/E

**F** permeability
- Control
- RAMP2 O/E

**G** Control  H$_2$O$_2$ (-)
**H** RAMP2 O/E

**I** Control  H$_2$O$_2$ (+)
**J** RAMP2 O/E

**K** Relative area of tight-junction
- Control
- RAMP2 O/E
H$_2$O$_2$ (-)    H$_2$O$_2$ (+)

**L**
VEGF    eNOS    CDN5
Relative gene expression
- Control
- RAMP2 O/E

A    A+L    L
A    A+L    L
A    A+L    L

VEGF    eNOS    CDN5
A    A+P    P
A    A+P    P
A    A+P    P

A:     AM 10$^{-7}$M
A+L:  AM+LY294002 10$^{-6}$M
A+P:  AM+PKAinhibitor 10$^{-6}$M

**Figure 4**

Establishment and functional analysis of the RAMP2O/E line. (**A**) Plasmid vector used to overexpress RAMP2 (see Methods). (**B**) Western blot analysis of the membrane protein fraction from RAMP2O/E cells showing expression of the transfected gene. (**C–E**) Capillary formation by EAhy926 cells on Matrigel. RAMP2O/E cells or control ECs were cultured in 24-well culture plates coated with Matrigel in medium containing $10^{-7}$ M AM, and capillary formation was monitored microscopically. (**C**) Capillary area relative to day-1 cell surface area. RAMP2O/E cells exhibited greater angiogenesis than control. $n = 8$ per group. (**D** and **E**) Representative photomicrographs of RAMP2O/E and control cells. (**F**) In vitro vascular permeability assay (see Methods). The permeability of the monolayer, assessed using a fluorescence microplate reader, is expressed relative to control at 5 min. RAMP2O/E cells showed significantly lower permeability than control ECs. $n = 10$ per group. *$P < 0.05$, **$P < 0.01$ vs. control. (**G–J**) Immunostaining of ZO-1. ECs were cultured until confluent on chamber slides in the presence of $10^{-7}$ M AM. Two hours after treatment with 0.5 mM $H_2O_2$, the cells were immunostained using anti–ZO-1 antibody and Hoechst 33342. (**K**) Comparison of the tight junctions illustrated by the immunostaining in **G–J**. Tight junctions were better preserved after $H_2O_2$ treatment in RAMP2O/E cells than control ECs. **$P < 0.01$ vs. $H_2O_2$-treated control; comparison in 4 microscopic fields each from 3 independent experiments. (**L**) Quantitative real-time PCR analysis of gene expression in ECs cultured on Matrigel. Values are relative to control ECs treated with $10^{-7}$ M AM. RAMP2O/E cells showed stronger expression of VEGF, eNOS, and CDN5 than control cells; this effect was blocked by LY294002 ($10^{-6}$ M) or a PKA inhibitor ($10^{-6}$ M). $n = 6$ per group. ##$P < 0.01$ and #$P < 0.05$ vs. AM-treated control. **$P < 0.01$ and *$P < 0.05$ vs. AM-treated RAMP2O/E. Scale bars: 50 μm (**D** and **E**); 10 μm (**G–J**).

angiogenic effect was greatly diminished in explants from *RAMP2*$^{+/-}$ mice (Figure 5, B–E). Similarly, in Matrigel plug assays, *RAMP2*$^{+/-}$ mice showed reduced neovascularization in response to stimulation with bFGF (Figure 5, F and G). We also cultured tissue from the aorta-gonad-mesonephros (AGM) regions of E10.5 embryos, which were plated on mouse OP9 stromal cells to promote angiogenesis. We found that there was substantially less development of a vascular network in tissue from *RAMP2*$^{-/-}$ than WT mice (Figure 5, H and I).

*Enhanced vascular permeability in adult RAMP2*$^{+/-}$ *mice.* Based on the findings presented thus far, we hypothesized that the AM-RAMP2 system regulates vascular stability in adults as well as during development, which we tested by analyzing vascular permeability in adult *RAMP2*$^{+/-}$ mice. We initially generated a footpad edema model by subcutaneously injecting λ-carrageenan, a sulfated high-MW polygalactan. As expected, *RAMP2*$^{+/-}$ mice showed greater swelling than did WT mice (Figure 6A). We then directly measured vascular permeability using a skin edema model. Mice were injected with FITC-BSA via the tail vein as a tracer of vascular permeability, after which serum exudation caused by subcutaneous injection of histamine was measured using a fluorescence microplate reader. As shown in Figure 6B, *RAMP2*$^{+/-}$ mice exhibited greater vascular permeability than did WT mice.

Finally, to prove that the capacity of the AM-RAMP2 system to regulate vascular permeability could in fact make it a useful therapeutic target, we generated a brain edema model in which edema was caused by injuring the brain using a liquid nitrogen–cooled

copper probe. Twenty-four hours after the injury, *RAMP2*$^{+/-}$ mice showed greater vascular permeability than did WT mice (Figure 6C), which suggests that the AM-RAMP2 system is important for maintenance of the blood-brain barrier.

## Discussion

The mechanism by which a stable and functional vascular network is generated and regulated by humoral factors is still not fully understood. For example, VEGF alone is insufficient for stable vessel formation (36) and presents major disadvantages for thera-
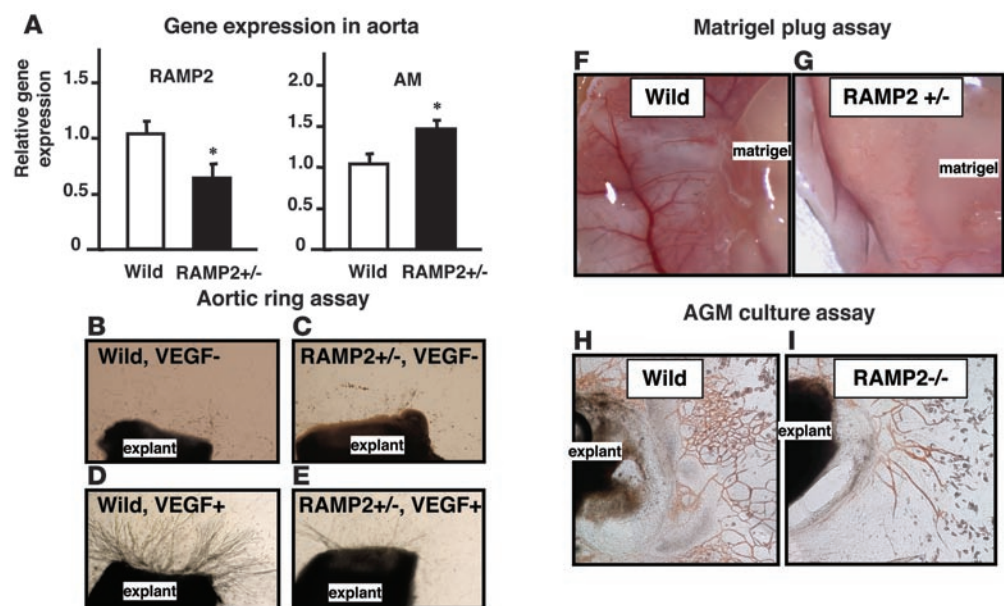


**Figure 5**

Reduced responses to angiogenic stimuli in adult *RAMP2*$^{+/-}$ mice. (**A**) Gene expression in aortas from 8-week-old WT and *RAMP2*$^{+/-}$ mice. Quantitative real-time PCR analysis of total RNA extracted. In *RAMP2*$^{+/-}$ mice, RAMP2 expression was about half that in WT mice, while AM expression was significantly upregulated. $n = 6$ per group. (**B–E**) Aortic ring assay. Representative photomicrographs of 7-day collagen gel cultures of aortas from 8-week-old mice (see Methods). Aortic explants from WT and *RAMP2*$^{+/-}$ mice were cultured in the absence or presence of VEGF (50 ng/ml), and capillaries sprouting from the edges of the rings were analyzed. The aortic explants from *RAMP2*$^{+/-}$ mice showed diminished angiogenesis. $n = 6$ per group. (**F** and **G**) Matrigel angiogenesis assay (see Methods). Representative photomicrographs showing angiogenesis in response to injected Matrigel. Capillary formation toward the Matrigel was greatly reduced in *RAMP2*$^{+/-}$ (**G**) compared with WT (**F**). $n = 6$ per group. (**H** and **I**) In vitro culture of AGM explant (see Methods). Representative photomicrographs showing the vascular network formation from the tissue cultured AGM region of E10.5 WT (**H**) and *RAMP2*$^{-/-}$ embryos (**I**). Vascular network formation was diminished in *RAMP2*$^{-/-}$ mice. $n = 4$ per group.
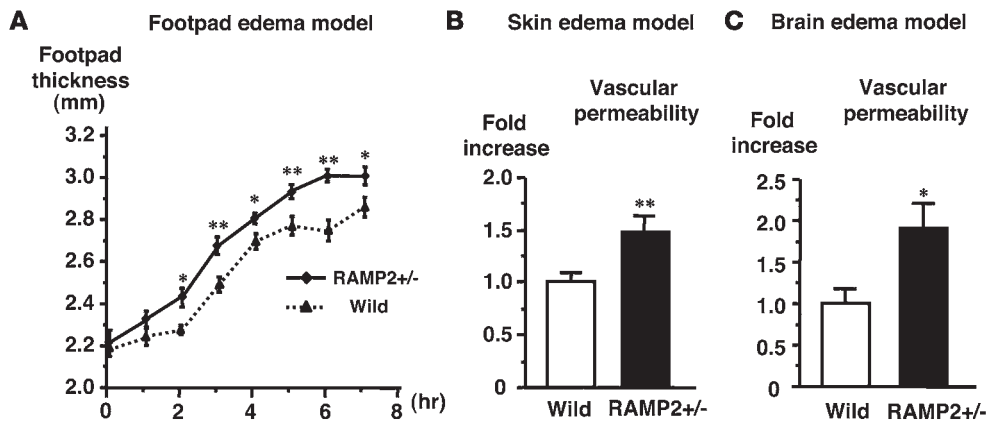
**Figure 6**
In vivo vascular permeability assay. (**A**) Footpad edema model. λ-Carrageenan was injected into the footpad of 8-week-old *RAMP2⁺/⁻* and WT mice to induce edema for the evaluation of vascular permeability in adult mice; swelling of the footpad was measured hourly using a thickness gauge. *RAMP2⁺/⁻* mice showed significantly greater swelling than WT mice. *n* = 12 per group. **$P < 0.01$, *$P < 0.05$ vs. WT. (**B**) Skin edema model (see Methods). Fluorescence intensity was measured using a fluorescence microplate reader. Permeability levels are presented relative to WT. *RAMP2⁺/⁻* mice (*n* = 8) showed significantly greater vascular permeability than WT mice (*n* = 13). **$P < 0.01$ vs. WT. (**C**) Brain edema model (see Methods). Vascular permeability in *RAMP2⁺/⁻* mice (*n* = 12) is presented relative to that in WT mice (*n* = 10). *RAMP2⁺/⁻* mice showed significantly greater vascular permeability than WT mice. *$P < 0.05$ vs. WT.

peutic angiogenesis, in that it increases vascular permeability and may exacerbate arteriosclerosis.

Studies of gene-targeted mice have led to the identification of angiogenic factors that had not previously been recognized for their angiogenic properties. AM was originally identified as a vasodilator, although it is now known to possess a variety of biological activities. Indicative of AM's novel angiogenic properties is our previous finding that *AM⁻/⁻* embryos die in utero due to hemorrhage and edema resulting from abnormalities of vascular development (14). We also showed previously that exogenous administration of AM enhances angiogenesis in ischemic tissues in adults, and therapeutic application of AM is much anticipated (25). Gene-targeted mice also provide information about the fundamental roles played by AM during the multistep process of angiogenesis. It is noteworthy, for instance, that *AM⁻/⁻* embryos die at a relatively late stage of development (E13.5–E14.5) compared with KO mice lacking other substances classified as angiogenic factors. This suggests that the vasculature does develop in *AM⁻/⁻* mice, but its fragile structure is likely disrupted after the start of circulation. It also clearly shows that AM is essential not only for angiogenesis, but also for vascular integrity.

As with other growth factors, the clinical applicability of AM has 2 serious limitations: AM is a peptide with a short half-life in the bloodstream, and the cost of the recombinant protein makes its use in the treatment of chronic diseases impractical. This prompted us to focus on AM's receptor system. McLatchie et al. showed that AM signaling is regulated by a unique control system (28). The main body of the AM receptor is thought to be CRLR, a 7–transmembrane domain GPCR. CRLR associates with 1 of 3 subtypes of RAMP, which determines the affinity of CRLR for its ligands. By generating RAMP2-specific KO mice, we have been able to demonstrate that RAMP2 is the key determinant of AM's function during vascular development. In our *RAMP2⁻/⁻* mice, CRLR and the other RAMPs were preserved; nevertheless, deletion of RAMP2 was sufficient to reproduce the phenotypes of the *AM⁻/⁻* genotype. Our finding that AM expression was upregulated in *RAMP2⁻/⁻* embryos

just before their death further confirms that RAMP2 is essential for AM signaling during vascular development.

In both *AM⁻/⁻* and *RAMP2⁻/⁻* embryos, vascular fragility ultimately leads to hemorrhage and edema. Notably, however, the systemic edema was much more severe in *RAMP2⁻/⁻* mice. Edema was sometimes detected in *AM⁻/⁻* mice, but its severity varied. Moreover, administration of recombinant AM to crossbred *AM⁺/⁻* females increased the survival rate of *AM⁻/⁻* embryos at E14.5 (14), suggesting that maternally supplied AM partially compensates for the lack of embryonic AM expression. By contrast, *RAMP2⁻/⁻* mice cannot express a functional AM receptor in their vasculature and thus can not respond to maternal AM.

We found that neovascularization was diminished and vascular permeability was increased in adult *RAMP2⁺/⁻* mice, which showed reduced expression of RAMP2. We also found that *RAMP2⁺/⁻* mice had higher BP than did their WT littermates, which confirms that RAMP2 continues to be a crucial determinant of vascular function in the adult. Interestingly, we also found that the edema developed by *RAMP2⁺/⁻* mice in various disease models was more severe than that in WT mice, suggesting the AM-RAMP2 system could be an attractive therapeutic target for treating the edema often associated with vascular regenerative therapies, brain trauma, and infarction. In that regard, it is noteworthy that we were able to modulate the vascular function of AM by modulating RAMP2. Using RAMP2O/E cells, we clearly showed that by upregulating RAMP2 signaling, we could enhance capillary formation, firm up tight junctions, and reduce vascular permeability. RAMP2O/E cells were also resistant to apoptosis. Thus, RAMP2 could be a therapeutic target by which to manipulate the vascular functions of AM.

By contrast, RAMP3O/E cell lines did not show either enhanced angiogenesis or improved vascular stability, although RAMP3 has previously been shown to work with CRLR to function as another AM receptor (37). Furthermore, our finding that RAMP3 was expressed at WT levels in *RAMP2⁻/⁻* mice confirmed that RAMP3 cannot compensate for the absence of RAMP2 during vascular development. Consistent with the distinctly different physiologi-

cal roles played by RAMP2 and RAMP3, *RAMP3*^{−/−} mice live apparently normally until old age (38). In addition, whereas RAMP2 and CRLR are downregulated in an endotoxemia model, RAMP3 is markedly upregulated (39), and it has been suggested that RAMP3 may be involved in post-endocytic receptor trafficking, as it presents a PDZ type I domain (40).

Signal transduction via GPCRs and the regulation of their function has long attracted the interest of many researchers. Indeed, about 40% of the drugs in clinical use today target GPCRs. We suggest that RAMP2 is an alternative therapeutic target by which to affect CRLR function. Because RAMP2 is a low-MW protein, structural analysis and the synthesis of specific agonists or antagonists are much more realistic for RAMP2 than for 7–transmembrane domain GPCRs, which has proven difficult. Moreover, because RAMP2 determines the vascular functions of AM, it would be expected that greater specificity would be achieved by targeting RAMP2 than by targeting CRLR, which can also function as a receptor for other ligands. In that context, our findings provide a clear basis for the development of drugs to modulate RAMP2 and, thereby, the vascular effects of AM.

## Methods

*Generation of RAMP2 KO mice.* KO mice were generated as described previously (14, 16, 41, 42). Briefly, a plasmid-targeting vector was constructed to insert loxP sites encompassing exons 2–4 of *RAMP2* and the neomycin resistance gene, after which the plasmid was linearized and introduced into Bruce 4 embryonic stem cells by electroporation. Homologous recombinants were identified, and 2 independently targeted clones were injected into BALB/c blastocysts to generate chimeric mice. Male chimeras were crossbred with C57BL/6 females, and germline transmission was verified by Southern blot analysis. After obtaining heterozygotic floxed RAMP2 mice, we crossbred them with CAG-Cre mice to delete exons 2–4 of the *RAMP2* gene. The deletion of RAMP2 was certified by Southern blot analysis. The Cre gene was then removed from the line by backcrossing with C57BL/6 mice. All experiments were performed in accordance with the Declaration of Helsinki and were approved by the Shinshu University Ethics Committee for Animal Experiments.

*In situ hybridization.* In situ hybridization was performed as described previously (43). cRNAs were prepared from linearized cDNA templates of murine RAMP2 (ACACTTTGCGAACTGCTCCCTGGTGCAGCCCACCTTCTCTGATCCCCCAGAGGATGTGCTCCTGGCCATGATCATAGCCCCCATCTGCCTCATCCCGTTCCTTGTTACTCTTGTGGTGTGGAGGAGTAAAGACAGCGATGCCCAGGCCTAGGGTCCATTTCTCAGCAGCCATTTTTCCCCCCTTTTCCCTGCTGGAACCAGGAATGGCGCTCCTCCCCTCCCTACCCACTTACTCTCATCCTTCCCACAGACCTGTGGATTGGTGGAAATGGCAGCAAAGGGGACTCACGACACAATG) to generate antisense and sense probes. The cRNA transcripts were synthesized according to the manufacturer's instructions (Ambion).

*Histological examination.* Whole embryos, yolk sac and placenta, were fixed in 4% phosphate-buffered paraformaldehyde (pH 7.2), embedded in paraffin, and cut into 4-μm sections for histological examination. Some yolk sacs were used for immunohistochemical staining with anti-mouse CD31 antibody (BD Biosciences − Pharmingen) to visualize blood vessels. Samples were stained with a Histofine MOUSESTAIN KIT (Nichirei Biosciences) and DAB chromogen and counterstained with methyl green. Apoptosis was visualized in green fluorescence using the TUNEL method with an Apoptosis In Situ Detection Kit (Chemicon) and nuclei were stained with Hoechst 33342. To evaluate the aortic wall structure, immunohistochemical staining was performed using anti-mouse type IV

collagen antibody (Collaborative Research), phalloidin, and DAPI (Roche Diagnostics). Confocal microscopic observation was then carried out using a Leica TCS-SP2 laser scanning microscope.

*Transmission electron microscopy.* Specimens were fixed in 2% glutaraldehyde (pH 7.2) and 4% osmium tetroxide, embedded in epoxy resin (Epok) 812 (Oken Shoji Co.), cut into ultrathin sections, double-stained with uranyl acetate and lead citrate, and examined by electron microscopy (JEM-1010; Jeol).

*Quantitative real-time PCR analysis.* Total RNA was extracted from tissues or cells using TRIZOL Reagent (Invitrogen), after which it was treated with DNA-Free (Ambion) to remove contaminating DNA and subjected to reverse transcription using an Omniscript RT kit (QIAGEN) with random primers (Invitrogen). Quantitative real-time RT-PCR analysis was carried out using an ABI PRISM 7300 Sequence Detection System (Applied Biosystems) with SYBR Green (Toyobo) or TaqMan probe, and values were normalized to 18S rRNA (TaqMan Ribosomal RNA Control Reagents VIC Probe; Applied Biosystems). The primers and probes used were as follows: mouse AM (mAM) forward, 5′-CTACCGCCAGAGCATGAACC-3′; mAM reverse, 5′-GAAATGTGCAGGTCCCGAA-3′; mAM probe, 5′-CCCGCAGCAATGGATGCCG-3′; mRAMP2 forward, 5′-GCAGCCCACCTTCTCTGATC-3′; mRAMP2 reverse, 5′-AACGGGATGAGGCAGATGG-3′; mRAMP2 probe, 5′-CCCAGAGGATGTGCTCCTGGCCAT-3′; mRAMP3 forward, 5′-TGCAACGAGACAGGGATGC-3′; mRAMP3 reverse, 5′-GCATCATGTCAGCGAAGGC-3′; mRAMP3 probe, 5′-AGAGGCTGCCTCGCTGTGGGAA-3′; mCRLR forward, 5′-AGGCGTTTACCTGCACACACT-3′; mCRLR reverse, 5′-CAGGAAGCAGAGGAAACCCC-3′; mCRLR probe, 5′-ATCGTGGTGGCTGTGTTTGCGGAG-3′; mVE-cadherin forward: 5′-GGTGGCCAAAGACCCTGAC-3′; mVE-cadherin reverse, 5′-ACTGGTCTTGCGGATGGAGT-3′; mCDN5 forward, 5′-GCCTTCCTGGACCACAACA-3′; mCDN5 reverse, 5′-ACGACATCCACAGCCCCTT-3′; mCDN5 probe, 5′-CGTGACGGCGCAGACGACTTG-3′; mα2 type IV collagen forward, 5′-CACAACATCAACGATCCACCC-3′; mα2 type IV collagen reverse, 5′-GAACCCCATGATGCCTTCCT-3′; mα2 type IV collagen probe, 5′-AGCAAGGGATACCCGGCGTAATCTCA-3′; human VEGF (hVEGF) forward, 5′-TACCTCCACCATGCCAAGTG-3′; hVEGF reverse, 5′-GTGATGATTCTGCCCTCCTCC-3′; heNOS forward, 5′-AGATCTCCGCCTCGCTCAT-3′; heNOS reverse, 5′-AGCCATACAGGATTGTCGCC-3′; hCDN5 forward, 5′-AGGCGTGCTCTACCTGTTTTG-3′; hCDN5 reverse, 5′-AACTCGCGGACGACAATGTT-3′.

The PI3K inhibitor LY294002 ($10^{-6}$ M) and a PKA inhibitor (14-22 cell permeable PKA inhibitor; $10^{-6}$ M) were obtained from Calbiochem.

*Establishment of the RAMP2O/E line.* The RAMP2O/E cell line was created using EAhy926 ECs, an immortal, clonally pure, human EC line obtained through hybridization of HUVECs and line A 549/8 lung carcinoma cells (kindly provided by C.J. Edgell, University of North Carolina, Chapel Hill, North Carolina, USA). EAhy926 human ECs were cultured in DMEM (Invitrogen) supplemented with 10% FBS (EQUITECH-BIO INC.). Full-length hRAMP2 cDNA was obtained from the UMR cDNA Resource Center (University of Missouri–Rolla). hRAMP2 (580 bp) labeled with HA-tag was inserted into the cloning site of pcDNA3.1⁺ vector (Invitrogen), which was then linearized and transfected into EAhy926 cells using Effectene transfection reagent (QIAGEN). Four cell lines overexpressing RAMP2 were then cloned from G418-resistant (400 μg/ml) colonies. EAhy926 cells transfected with empty pcDNA3.1⁺ vector served as controls.

*Capillary formation on Matrigel.* RAMP2O/E cells or control ECs were cultured on 24-well culture plates coated with Matrigel (BD) in medium containing $10^{-7}$ M recombinant hAM (Peptide Institute), and capillary formation was monitored microscopically. Photomicrographs were taken of 2 different fields in each well, and the degree of capillary formation was evaluated by quantification of the total capillary area in each field using

NIH Image software. Capillary area was then presented relative to the cell surface area of the control cells on day 1.

*In vitro vascular permeability assay*. To assay vascular permeability in vitro, we used a permeability chamber consisting of a 24-well tissue culture plate with cell culture inserts. The inserts contained a transparent polyethylene membrane with a high density of symmetrical pores (1 μm in diameter) that permitted high rates of basolateral diffusion. RAMP2O/E and control cells were seeded onto collagen-coated (Cellmatrix Type I-C; Nitta Gelatin Inc.) inserts, after which confluent endothelial monolayers that occluded the membrane pores were allowed to form over several days. The cell monolayers were then treated with 10 ng/ml VEGF, after which 13.3 mg/ml Dextran FITC Conjugate (MW 70,000; Research Organics) was added on top of the cells. The permeability of the monolayer was then assessed by measuring the fluorescence of the solution in the wells using a Multi-Detection Microplate Reader (POWERSCAN HT; DS Pharma Biomedical). The excitation and emission wavelengths were 485 nm and 530 nm, respectively.

*Structure of tight junction after cell injury*. EAhy926 ECs were cultured until confluent on chamber slides in DMEM containing $10^{-7}$ M AM and then exposed to 0.5 mM $H_2O_2$. Two hours after the $H_2O_2$ treatment, the cells were immunostained with anti–ZO-1 antibody (BD Biosciences — Pharmingen) and the nucleus-specific dye Hoechst 33342 (Sigma-Aldrich) and observed under a confocal microscope.

*Aortic ring assay*. After mice were killed with an overdose of anesthetic, the thoracic aorta was dissected from the posterior mediastinum, placed in serum-free EBM-2 endothelial basal medium (Cambrex), and cleaned of blood and fibroadipose tissue under a stereoscopic microscope using fine forceps and scissors. The vessel was then cut into 1-mm-long rings, which were subjected to 8 consecutive washes with serum-free EBM-2. The aortic rings were then embedded in thick collagen gel (Cellmatrix Type I-A; Nitta Gelatin Inc.) and cultured for 7 days, with or without recombinant hVEGF (50 ng/ml; R&D Systems) supplement. The capillaries that sprouted from the edges of the rings were analyzed (44).

*Matrigel assay*. After mice were anesthetized, 500 μl Matrigel (BD) containing 100 ng recombinant hbFGF (Wako) was injected subcutaneously into the dorsal region using a 25-gauge needle and permitted to solidify. Seven days later, the mice were killed with an overdose of anesthetic, the skin around the injected sites was incised, and the angiogenic response to the implanted Matrigel was analyzed.

*AGM culture*. Tissue culture of the AGM regions was carried out as described previously (45). The AGM regions were dissected from E10.5 embryos and plated on mouse OP9 stromal cells cultured on a 24-well dish. After 5 days of culture, capillaries growing from the AGM explant were stained with anti-CD31 antibody.

*Footpad edema model*. Vascular permeability leading to mouse footpad edema was assayed as described previously (46). Briefly, 20 μl of 0.01 g/ml λ-carrageenan (Wako) was injected subcutaneously into the footpads of 8-week-old mice, after which the swelling of the footpad was monitored using a thickness gauge (resolution, 1 μm).

*Skin edema model*. Vascular permeability leading to mouse skin edema was assayed as described previously (47). Mice were injected via the tail vein with 0.2 ml of 1.5% FITC-BSA (15 mg/ml) in isotonic Tyrode solution, which served as a tracer of vascular permeability. Thereafter, serum exudation was induced by subcutaneous injection of histamine (1 μg/100 μl/site) into the shaved dorsal skin. Thirty minutes later, the injected sites in the dorsal skin were removed as circular patches and put into the wells of a 24-well culture plate. Formamide (1 ml) was then added to each well and incubated at 50°C for 2 h, after which the fluorescence intensity in each well was measured using a Multi-Detection Microplate Reader; the excitation and emission wavelengths were 485 nm and 530 nm, respectively.

*Brain edema model (cold lesion model)*. Mice were mounted in a stereotaxic frame (Narishige), after which the scalp was incised, subcutaneous tissue was retracted from the bone, and the skull was exposed. Using a drill, a circular craniotomy was then carried out over the right parietal cortex, extending from the lambda suture to bregma, and the resultant bone flap was lifted off to expose the underlying dura. The cold lesion was made using a copper cylinder (3 mm in diameter) that had been precooled with liquid nitrogen. The metal probe was lowered quickly onto the surface of the intact dura over the parietotemporal cortex under microscopic control and pressed down to a depth of 1 mm for 30 seconds (48).

To quantify the vascular permeability of brain vessels, 0.2 ml of sodium fluorescein at a concentration of 6 mg/ml in PBS was injected via the tail vein 24 hours after making the cold lesions. Thirty minutes later, the mice were anesthetized and perfused with PBS (20 ml) via the left cardiac ventricle to remove the fluorescent tracer from the vascular bed. To assess their fluorescence, brain hemispheres were homogenized in 0.5 M borate buffer (pH 10) and centrifuged (800 *g*) for 15 min at 4°C, after which the supernatant was added to 1.2 ml of ethanol to precipitate the proteins. The samples were again centrifuged, and the fluorescence in the supernatant was measured using a Multi-Detection Microplate Reader (49); the excitation and emission wavelengths were 330 nm and 485 nm, respectively.

*Statistics*. Quantitative values are expressed as mean ± SE. Student's *t* tests were used to determine significant differences. Values of $P < 0.05$ were considered significant.

Address correspondence to: Takayuki Shindo, Department of Organ Regeneration, Shinshu University Graduate School of Medicine, 3-1-1 Asahi, Matsumoto 390-8621, Japan. Phone: 81-263-37-3192; Fax: 81-263-37-3437; E-mail: t-shindo@sch.md.shinshu-u.ac.jp.

1. Kitamura, K., et al. 1993. Adrenomedullin: a novel hypotensive peptide isolated from human pheochromocytoma. *Biochem. Biophys. Res. Commun.* **192**:553–560.
2. Michibata, H., et al. 1998. Autocrine/paracrine role of adrenomedullin in cultured endothelial and mesangial cells. *Kidney Int.* **53**:979–985.
3. Kitamura, K., et al. 1994. Immunoreactive adrenomedullin in human plasma. *FEBS Lett.* **341**:288–290.
4. Jougasaki, M., et al. 1995. Renal localization and actions of adrenomedullin: a natriuretic peptide. *Am. J. Physiol.* **268**:F657–F663.
5. Nishikimi, T., and Matsuoka, H. 2005. Cardiac adrenomedullin: its role in cardiac hypertrophy and heart failure. *Curr. Med. Chem. Cardiovasc. Hematol. Agents.* **3**:231–242.
6. Samson, W.K., Murphy, T., and Schell, D.A. 1995. A novel vasoactive peptide, adrenomedullin, inhibits pituitary adrenocorticotropin release. *Endocrinology.* **136**:2349–2352.
7. Petrie, M.C., Hillier, C., Morton, J.J., and McMurray, J.J. 2000. Adrenomedullin selectively inhibits angiotensin II-induced aldosterone secretion in

humans. *J. Hypertens.* **18**:61–64.

8. Isumi, Y., Kubo, A., Katafuchi, T., Kangawa, K., and Minamino, N. 1999. Adrenomedullin suppresses interleukin-1beta-induced tumor necrosis factor-alpha production in Swiss 3T3 cells. *FEBS Lett.* **463**:110–114.

9. Shimosawa, T., et al. 2002. Adrenomedullin, an endogenous peptide, counteracts cardiovascular damage. *Circulation.* **105**:106–111.

10. Shimosawa, T., et al. 2003. Deficiency of adrenomedullin induces insulin resistance by increasing oxidative stress. *Hypertension.* **41**:1080–1085.

11. Kano, H., et al. 1996. Adrenomedullin as a novel antiproliferative factor of vascular smooth muscle cells. *J. Hypertens.* **14**:209–213.

12. Miyashita, K., et al. 2003. Adrenomedullin promotes proliferation and migration of cultured endothelial cells. *Hypertens. Res.* **26**(Suppl.):S93–S98.

13. Iwasaki, H., Eguchi, S., Shichiri, M., Marumo, F., and Hirata, Y. 1998. Adrenomedullin as a novel growth-promoting factor for cultured vascular smooth muscle cells: role of tyrosine kinase-mediated mitogen-activated protein kinase activation. *Endocrinology.* **139**:3432–3441.

14. Shindo, T., et al. 2001. Vascular abnormalities and elevated blood pressure in mice lacking adrenomedullin gene. *Circulation.* **104**:1964–1971.

15. Shindo, T., et al. 2000. Hypotension and resistance to lipopolysaccharide-induced shock in transgenic mice overexpressing adrenomedullin in their vasculature. *Circulation.* **101**:2309–2316.

16. Oh-hashi, Y., et al. 2001. Elevated sympathetic nervous activity in mice deficient in alphaCGRP. *Circ. Res.* **89**:983–990.

17. Niu, P., et al. 2004. Protective effects of endogenous adrenomedullin on cardiac hypertrophy, fibrosis, and renal damage. *Circulation.* **109**:1789–1794.

18. Niu, P., et al. 2003. Accelerated cardiac hypertrophy and renal damage induced by angiotensin II in adrenomedullin knockout mice. *Hypertens. Res.* **26**:731–736.

19. Nishimatsu, H., et al. 2002. Role of endogenous adrenomedullin in the regulation of vascular tone and ischemic renal injury: studies on transgenic/knockout mice of adrenomedullin gene. *Circ. Res.* **90**:657–663.

20. Imai, Y., et al. 2002. Resistance to neointimal hyperplasia and fatty streak formation in mice with adrenomedullin overexpression. *Arterioscler. Thromb. Vasc. Biol.* **22**:1310–1315.

21. Yamamoto, H., et al. 2007. Adrenomedullin insufficiency increases allergen-induced airway hyperresponsiveness in mice. *J. Appl. Physiol.* **102**:2361–2368.

22. Kurihara, H., Shindo, T., Oh-Hashi, Y., Kurihar, Y., and Kuwaki, T. 2003. Targeted disruption of adrenomedullin and alphaCGRP genes reveals their distinct biological roles. *Hypertens. Res.* **26**(Suppl.):S105–S108.

23. Nishimatsu, H., et al. 2003. Endothelial responses of the aorta from adrenomedullin transgenic mice and knockout mice. *Hypertens. Res.* **26**(Suppl.):S79–S84.

24. Aoki-Nagase, T., et al. 2002. Attenuation of antigen-induced airway hyperresponsiveness in CGRP-deficient mice. *Am. J. Physiol. Lung Cell Mol. Physiol.* **283**:L963–L970.

25. Iimuro, S., et al. 2004. Angiogenic effects of adrenomedullin in ischemia and tumor growth. *Circ. Res.* **95**:415–423.

26. Fujii, T., et al. 2005. Adrenomedullin enhances therapeutic potency of bone marrow transplantation for myocardial infarction in rats. *Am. J. Physiol. Heart Circ. Physiol.* **288**:H1444–H1450.

27. Nagaya, N., et al. 2005. Adrenomedullin: angiogenesis and gene therapy. *Am. J. Physiol. Regul. Integr. Comp. Physiol.* **288**:R1432–R1437.

28. McLatchie, L.M., et al. 1998. RAMPs regulate the transport and ligand specificity of the calcitonin-receptor-like receptor. *Nature.* **393**:333–339.

29. Kuwasako, K., Cao, Y.N., Nagoshi, Y., Kitamura, K., and Eto, T. 2004. Adrenomedullin receptors: pharmacological features and possible pathophysiological roles. *Peptides.* **25**:2003–2012.

30. Parameswaran, N., and Spielman, W.S. 2006. RAMPs: The past, present and future. *Trends Biochem. Sci.* **31**:631–638.

31. Morfis, M., Christopoulos, A., and Sexton, P.M. 2003. RAMPs: 5 years on, where to now? *Trends Pharmacol. Sci.* **24**:596–601.

32. Montuenga, L.M., Martinez, A., Miller, M.J., Unsworth, E.J., and Cuttitta, F. 1997. Expression of adrenomedullin and its receptor during embryogenesis suggests autocrine or paracrine modes of action. *Endocrinology.* **138**:440–451.

33. Montuenga, L.M., Mariano, J.M., Prentice, M.A., Cuttitta, F., and Jakowlew, S.B. 1998. Coordinate expression of transforming growth factor-beta1 and adrenomedullin in rodent embryogenesis. *Endocrinology.* **139**:3946–3957.

34. Bauer, J., et al. 1992. In vitro model of angiogenesis using a human endothelium-derived permanent cell line: contributions of induced gene expression, G-proteins, and integrins. *J. Cell Physiol.* **153**:437–449.

35. Edgell, C.J., Curiel, D.T., Hu, P.C., and Marr, H.S. 1998. Efficient gene transfer to human endothelial cells using DNA complexed to adenovirus particles. *Biotechniques.* **25**:264–268, 270–272.

36. Lee, R.J., et al. 2000. VEGF gene delivery to myocardium: deleterious effects of unregulated expression. *Circulation.* **102**:898–901.

37. Sexton, P.M., Albiston, A., Morfis, M., and Tilakaratne, N. 2001. Receptor activity modifying proteins. *Cell Signal.* **13**:73–83.

38. Dackor, R.T., Fritz-Six, K.L., Smithies, O., and Caron, K.M. 2007. Receptor activity modifying proteins 2 and 3 have distinct physiological functions from embryogenesis to old age. *J. Biol. Chem.* **282**:18094–18099.

39. Ono, Y., Okano, I., Kojima, M., Okada, K., and Kangawa, K. 2000. Decreased gene expression of adrenomedullin receptor in mouse lungs during sepsis. *Biochem. Biophys. Res. Commun.* **271**:197–202.

40. Bomberger, J.M., Parameswaran, N., Hall, C.S., Aiyar, N., and Spielman, W.S. 2005. Novel function for receptor activity-modifying proteins (RAMPs) in post-endocytic receptor trafficking. *J. Biol. Chem.* **280**:9297–9307.

41. Shindo, T., et al. 2000. ADAMTS-1: a metalloproteinase-disintegrin essential for normal growth, fertility, and organ morphology and function. *J. Clin. Invest.* **105**:1345–1352.

42. Shindo, T., et al. 2002. Kruppel-like zinc-finger transcription factor KLF5/BTEB2 is a target for angiotensin II signaling and an essential regulator of cardiovascular remodeling. *Nat. Med.* **8**:856–863.

43. Lyons, G.E., Schiaffino, S., Sassoon, D., Barton, P., and Buckingham, M. 1990. Developmental regulation of myosin gene expression in mouse cardiac muscle. *J. Cell Biol.* **111**:2427–2436.

44. Zhu, W.H., Iurlaro, M., MacIntyre, A., Fogel, E., and Nicosia, R.F. 2003. The mouse aorta model: influence of genetic background and aging on bFGF- and VEGF-induced angiogenic sprouting. *Angiogenesis.* **6**:193–199.

45. Hamaguchi, I., et al. 1999. In vitro hematopoietic and endothelial cell development from cells expressing TEK receptor in murine aorta-gonad-mesonephros region. *Blood.* **93**:1549–1556.

46. Sakurai, K., et al. 1997. Anti-inflammatory activity of superoxide dismutase conjugated with sodium hyaluronate. *Glycoconj. J.* **14**:723–728.

47. Yamaki, K., Takano-Ishikawa, Y., Goto, M., Kobori, M., and Tsushida, T. 2002. An improved method for measuring vascular permeability in rat and mouse skin. *J. Pharmacol. Toxicol. Methods.* **48**:81–86.

48. Hortobagyi, T., et al. 2000. A novel brain trauma model in the mouse: effects of dexamethasone treatment. *Pflugers Arch.* **441**:409–415.

49. Schoch, H.J., Fischer, S., and Marti, H.H. 2002. Hypoxia-induced vascular endothelial growth factor expression causes vascular leakage in the brain. *Brain.* **125**:2549–2557.